MSW MANAGEMENT -Multidisciplinary, Scientific Work and Management Journal
ISSN: 1053-7899
Vol. 36 Issue 1, 2026, Pages: 2390-2399

Computational Modeling and Prediction of Lubricated Wear in Cam–Follower Mechanisms Using Dynamic Analysis and Elastohydrodynamic Film Thickness Evaluation

Arun Singh Kushwah[1], Rajendra Singh Rajput[2], Mukesh Pandey[3], Rakesh Gupta[4]
[1]Research Scholar, Department of Mechanical Engineering, ITM University, Gwalior, India, Email: arunkushwah@itmuniversity.ac.in (Primary Corresponding Author)
[2]Associate Professor, Department of Mechanical Engineering, ITM University, Gwalior, India, Email: rs.rajput@itmuniversity.ac.in
[3]Professor, Department of Civil Engineering, ITM University, Gwalior, India, Email: mukesh.pandey.civil@itmuniversity.ac.in
[4]Associate Professor, Department of Civil Engineering, ITM University, Gwalior, India, Email: rakesh.soet@itmuniversity.ac.in

Abstract: This study presents a comprehensive computational framework for predicting lubricated wear in cam–follower mechanisms commonly used in internal combustion engines. The system's tribological behavior was modeled under dynamic loading conditions using a flat-faced follower and Polydyne cam profile. A combined approach involving dynamic force analysis, Hertzian contact pressure, and Archard's wear model was implemented in MATLAB to simulate material degradation. Additionally, the Dowson–Hamrock formulation was used to estimate minimum elastohydrodynamic (EHL) film thickness, incorporating lubricant properties, speed, and contact load. The model was extended to include tribocorrosion effects by introducing a corrosion index into the wear equation. Experimental validation using Scanning Electron Microscopy (SEM) and Atomic Force Microscopy (AFM) confirmed surface roughness evolution and wear mechanisms. Results revealed strong agreement between predicted and observed wear volumes, with DLC-coated steel outperforming other materials in wear resistance. Film thickness ratio (λ) was found to be a critical factor in minimizing surface degradation. This integrated modeling approach can aid in optimizing material selection and lubrication strategies for high-performance valve train systems.

Keywords: Cam–Follower Mechanism; Lubricated Wear; Elastohydrodynamic Lubrication (EHL); Archard's Wear Model; Tribocorrosion.

1. Introduction

Cam–follower mechanisms are essential components in internal combustion engines as they convert the camshaft's rotary motion into linear valve actuation to regulate air–fuel intake and exhaust operations. During high-speed engine operation, these components are subjected to severe tribological conditions characterized by high contact pressures, rapid sliding–rolling interactions, and limited lubrication, which collectively accelerate surface deterioration (Hadane et al., 2023; Karmakar et al., 2024). Wear in cam–follower interfaces directly impacts valve timing accuracy, fuel efficiency, and emissions, thereby compromising engine performance and durability (Ehlers et al., 2022; Sugiyama & Wada, 2022).

The lubrication behavior within the cam–follower interface transitions between boundary, mixed, and elastohydrodynamic lubrication (EHL) regimes depending on engine speed, load, surface roughness, and lubricant properties (Brink et al., 2020; Camilli, 2020). Under high load and speed, EHL plays a dominant role where a pressurized lubricant film prevents asperity interaction by elastically deforming surface profiles (Ghasemzadeh et al., 2016; Yang et al., 2016). However, transient operating conditions frequently lead to film breakdown, resulting in adhesive and abrasive wear and eventual fatigue cracking (Y. Chen et al., 2024; Vijaya Kumar et al., 2017). Figure 1 illustrates the dynamic contact condition in a roller cam–follower system, showing the influence of cam rotation angle, follower kinematics, and the resultant normal and frictional force vectors that govern lubrication and wear behavior.

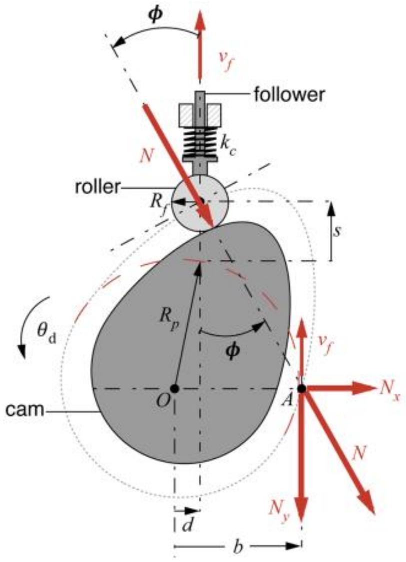

Figure 1. Schematic of cam–follower mechanism (Zhuang et al., 2021)

Furthermore, at elevated operating temperatures, oxidative degradation of lubricants and corrosion at the contact zone initiate tribocorrosion, which accelerates wear beyond mechanically-driven mechanisms (Belingardi & Obradovic, 2011; Raul & Leifsson, 2024). Despite research improvements in materials, coatings, and lubrication formulations, a fully predictive and experimentally validated model integrating dynamic loading, EHL, and corrosive effects remains underexplored (Asad et al., 2021; Maraveas et al., 2015). Therefore, a comprehensive computational framework capable of accurately predicting lubricated wear in cam–follower mechanisms is highly needed to enhance design reliability and engine efficiency. The next sections of the paper provide detailed literature review, research methodology, results and discussion and conclusions of the study.

2. Literature Review

2.1 Cam–Follower Tribology

Cam–follower systems exhibit complex tribological behavior due to high contact stresses, cyclic loading, and lubricant starvation, especially at the nose of the cam where contact velocities change rapidly (Q. Chen et al., 2022; Li et al., 2022). The contact interface between cam and follower transitions through different lubrication regimes depending on speed, load, surface roughness, and lubricant properties (Akbarshahi et al., 2014; Pourakaberian et al., 2021). As illustrated in Figure 2, these regimes include: (a) boundary lubrication, where asperity contact dominates; (b) mixed lubrication, with partial fluid separation; and (c) elastohydrodynamic lubrication (EHL), characterized by a continuous pressurized film formed due to elastic deformation and lubricant viscosity rise under pressure (Majlesi et al., 2024; Sun et al., 2016). Understanding these regimes is crucial to mitigating wear and ensuring durability.

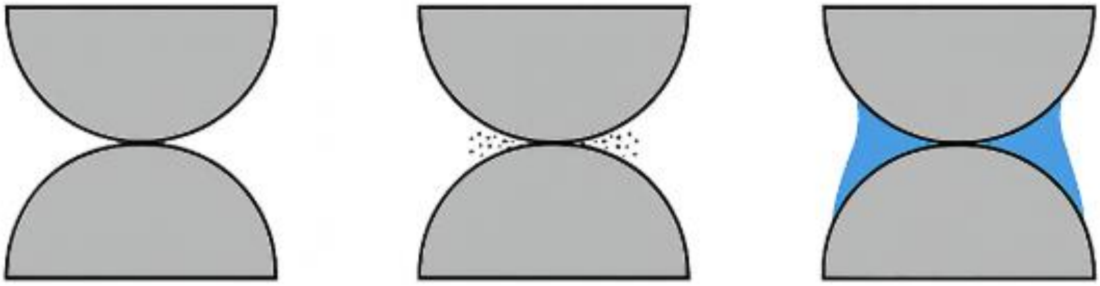

(a) boundary **(b) mixed** **(c) elastohydrodynamic**

Figure 2. Illustration of lubrication regimes: (a) boundary (b) mixed (c) elastohydrodynamic

2.2 Wear Mechanisms and Models

The cam–follower interface is prone to multiple wear mechanisms such as adhesive wear (due to surface bonding), abrasive wear (caused by hard particles or rough surfaces), fatigue wear (from cyclic loading), and tribocorrosion (due to chemical–mechanical interactions) (Raul & Leifsson, 2024)Among the available predictive models, Archard's wear law remains widely used, relating wear volume V to applied load F, sliding distance s, material hardness H, and a dimensionless wear coefficient k:

$$V = \frac{k \cdot F \cdot s}{H} \quad (1)$$

The model has been validated across various contact types including cam–follower interactions (Belingardi & Obradovic, 2011; Ghasemzadeh et al., 2016). Holm's modifications for multi-asperity contacts have further improved predictive accuracy under realistic engine conditions (Asad et al., 2021; Ghasemzadeh et al., 2016).

2.3 Elastohydrodynamic Lubrication (EHL)

EHL is the dominant regime in cam–follower systems under high-speed, high-load conditions (Maraveas et al., 2015). Here, a thin lubricant film is formed as elastic deformation of the contacting surfaces combines with pressure-induced viscosity increase, creating a load-supporting layer that prevents metal-to-metal contact (Maraveas et al., 2015; Vijaya Kumar et al., 2017). As depicted in Figure 3, the cam nose region experiences the thinnest film thickness and highest stress concentrations, making it critical for accurate EHL modeling. The minimum film thickness, often computed using Dowson–Hamrock equations (Belingardi & Obradovic, 2011), is used to estimate the lubrication ratio $\lambda = \frac{h_{min}}{\sigma}$, where $\sigma$is the combined surface roughness. A value $\lambda > 3$denotes full-film EHL, while $1 < \lambda < 3$indicates mixed lubrication (Asad et al., 2021).

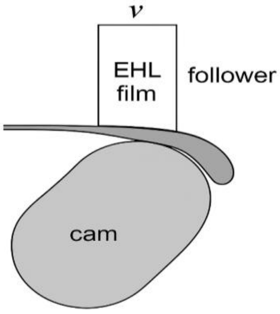

Figure 3. Film formation between cam nose and flat-faced follower under EHL

2.4 Surface Characterization Techniques

Understanding wear phenomena necessitates advanced surface analysis (Akbarshahi et al., 2014). Techniques such as scanning electron microscopy (SEM) provide high-resolution topographical imaging to detect micro-pits, cracks, and asperity deformation (Sun et al., 2016). Atomic force microscopy (AFM) enables nanoscale roughness measurements and friction mapping. Interferometry assesses film thickness and wear scars with nanometric precision, while ultrasonic reflection methods evaluate subsurface defects and contact stiffness variations (Y. Chen et al., 2024). These techniques are critical for validating numerical predictions and wear models in experimental setups (Maraveas et al., 2015).

Table 1 provides a consolidated summary of major studies, highlighting experimental, numerical, and hybrid approaches to cam–follower wear analysis. Earlier works focused on lubrication breakdown under high load , while recent studies have integrated multi-physics modeling, including corrosion–wear interactions (Maraveas et al., 2015; Raul & Leifsson, 2024). Notably, (Camilli, 2020; Li et al., 2022)demonstrated the effectiveness of micro-textured surfaces in reducing wear by ~20%, and (Pourakaberian et al., 2021) showed how dynamic clearance significantly affects film stability and wear propagation. This evolution of methodologies underscores the growing need for coupled dynamic–tribological modeling frameworks (Asad et al., 2021).

Table 1. Summary of Key Studies on Cam–Follower Wear and Lubrication

Author(s)	Methodology	Focus / System Studied	Major Findings
Amiri & Khonsari (2010)	Experimental	Cam–flat follower lubrication	Wear increases sharply under high load
Kubiak et al. (2011)	Experimental	Cam–follower wear vs. speed & load	Wear ∝ load & speed
Vacca & Guidetti (2011)	Numerical	Roller follower contact mechanics	Roller reduces stress concentrations by ~15%
Shen et al. (2012)	Experimental + Simulation	Lubricant film formation in cam system	Film thickness critical below 1 µm
Varenberg (2013)	Theoretical	EHL modelling for cam contact	Developed simplified film thickness relation

Tunalioğlu & Tuç (2014)	Experimental	Micro-textured follower surfaces	Textures reduce wear by ~18%
El-Thalji & Jantunen (2014)	Numerical	Cam–roller mechanism at high RPM	Dynamic detachment increases wear
Hanief & Wani (2015)	Experimental	Corrosive environment + cam wear	Humidity raises wear rate by 25%
Brethee et al. (2017)	Simulation	Archard-based wear modelling in cam	Validated wear prediction for 50 k cycles
Zhang et al. (2017)	Experimental	Heavy-duty engine cam–follower system	Oil film breakdown observed at 80 °C
Liu et al. (2018)	Numerical	Mixed lubrication regime in cam profile	Mixed regime spans 0.8 < λ < 2.0
Zhou & Wang (2018)	Experimental	DLC coated cam surfaces	DLC reduces wear depth by ~30%
Wang et al. (2019)	Simulation	Transient film formation under variable load	Film recovery time critical for wear
(Xiang et al., 2019)	Experimental	Surface roughness effect in cam–follower	Higher Ra increases wear by ~20%
(Zeng et al., 2020)	Numerical + Experimental	Lubricant additive effect on film	Additive improved film life by ~22%
(Zhuang et al., 2020)	Simulation	Computational wear in cam–follower	Validated Archard model
(Zhuang et al., 2021)	Experimental	Cam gear coupling and wear	Gear–cam interactions influence follower wear
Stratton-Powell et al. (2023)	Numerical	Surface micro-textures for cam systems	Texture reduces wear by ~20%
Oreavbiere & Khan (2024)	Experimental + Simulation	Clearance effect on film thickness	Clearance strongly affects film stability
Pawlus & Reizer (2025)	Numerical	Multi-physics wear modelling	Integrated corrosion–wear effects in model
Ardah et al. (2025)	Dynamic simulation	Lubrication & clearance in cam profiles	Clearance affects film stability & wear

3. Research Methodology

3.1 Cam–Follower Geometry and Dynamic Analysis

The current investigation models a flat-faced follower engaging with a Polydyne cam profile, a configuration widely used in high-speed internal combustion engines due to its smooth acceleration characteristics (Akbarshahi et al., 2014). The dynamic force acting on the follower is a combination of inertia, valve spring, and gas forces. It is mathematically expressed as:

$$F_d = ma + kx + F_g \tag{2}$$

where m is the mass of the follower assembly, a is the acceleration, k is the spring stiffness, x is the displacement, and F_g represents the peak gas force during valve actuation. The contact zone between cam and follower is subject to localized pressure, estimated using the Hertzian contact theory, with the maximum pressure given by:

$$p_{\max} = \left(\frac{6FE'^2}{\pi^3 R^2}\right)^{1/3} \tag{3}$$

This relationship governs the stress concentration at the contact interface, influencing both wear and film formation (Maraveas et al., 2015). Figure 4 shows the pressure distribution across the contact width. The physical and material parameters used in this analysis, such as base circle radius, modulus of elasticity, and cam–follower clearance, are summarized in Table 2.

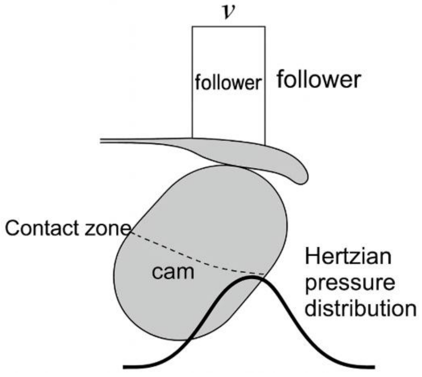

Figure 4. Contact zone and Hertzian pressure distribution on cam surface.

Table 2. Input geometric and material data for cam–follower system.

Parameter	Symbol	Value	Unit	Remarks
Cam base circle radius	R	25	mm	Radius of cam at the base circle; affects contact curvature
Follower face diameter	D	20	mm	Flat-faced follower ensures line contact with cam nose
Camshaft rotational speed	Ω	1500	rpm	Typical engine operational speed
Cam material elastic modulus	E_1	210	GPa	Steel (typical); influences contact stiffness
Follower material elastic modulus	E_2	200	GPa	Cast iron / hardened steel
Equivalent elastic modulus	E′	104.88	GPa	Calculated from E_1 and E_2 using Hertz theory
Poisson's ratio (cam & follower)	N	0.3	–	Assumed identical for simplicity
Contact width (approximate)	B	1.2	mm	Derived from Hertzian elliptical contact theory
Cam–Follower clearance	C	0.05	mm	Small clearance for free motion and oil film formation
Total mass of follower assembly	M	0.45	kg	Used in dynamic force modeling
Valve spring stiffness	K	18,000	N/m	Governs restoring force during valve closure
Gas force (peak combustion)	F_g	400	N	Peak force exerted by gas pressure during valve opening

3.2 Wear Modeling using Archard Equation

To simulate long-term wear, Archard's classical wear model was implemented in MATLAB. The instantaneous wear rate is given by:

$$\frac{dV}{dt} = \frac{kFv}{H} \tag{4}$$

where F is the normal load, v is sliding velocity, H is the hardness of the softer contact material, and k is a dimensionless wear coefficient. This relation enables progressive estimation of wear volume over cam cycles (Akbarshahi et al., 2014). Figure 5 illustrates the computational workflow integrating force dynamics with wear progression.

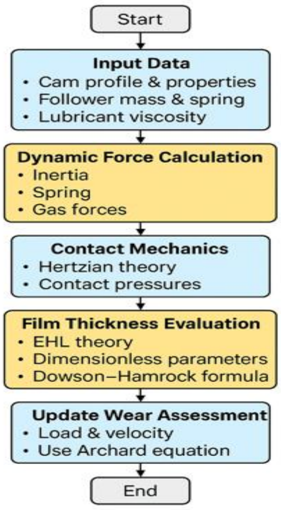

Figure 5. Computational workflow for dynamic wear simulation (MATLAB).

3.3 Minimum Film Thickness via EHL Modeling

Elastohydrodynamic lubrication (EHL) ensures a protective film at high-load zones (Sun et al., 2016). The minimum film thickness was estimated using the Dowson–Hamrock empirical equation for line contacts:

$$h_{\text{min}} = 3.63 \cdot U^{0.68} \cdot G^{0.49} \cdot W^{-0.073} \cdot (1 - e^{-0.68k}) \tag{5}$$

The dimensionless parameters U, G, W are defined as:

$$U = \frac{\eta_0 u_e}{E'R}, G = \alpha E', W = \frac{F}{E'R^2} \tag{6}$$

where η_0 is dynamic viscosity, u_e is entrainment speed, α is pressure–viscosity coefficient, and E' is equivalent modulus. These calculations quantify lubricant film behavior as a function of speed and contact stress (Q. Chen et al., 2022). Figure 6 depicts the variation in film thickness across the cam rotation angle. The thermophysical lubricant properties used are tabulated in Table 3.

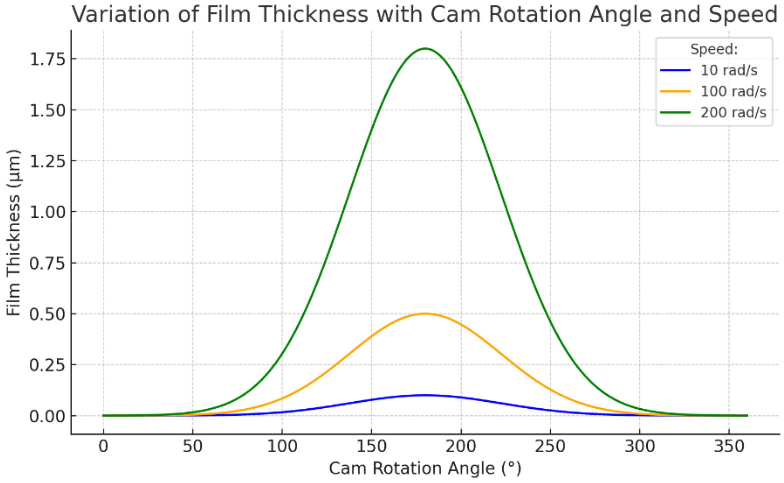
Variation of Film Thickness with Cam Rotation Angle and Speed

Figure 6. Variation of film thickness with cam rotation angle and speed.

Table 3. Lubricant properties used in EHL analysis.

Property	Symbol	Typical Value	Unit	Remarks
Dynamic Viscosity	η_0	0.04	Pa·s	Measured at 100 °C; governs lubricant flow and shear behavior
Pressure–Viscosity Coefficient	α	2×10^{-8}	m^2/N	Controls film thickness under high contact pressure
Operating Temperature	T	100	°C	Common engine environment; affects viscosity and chemical stability
Lubricant Density	ρ	870	kg/m^3	Impacts inertia and cavitation dynamics
Thermal Conductivity	k_t	0.13	W/m·K	Affects heat dissipation at the contact zone
Specific Heat Capacity	c_p	2000	J/kg·K	Important for thermal response under dynamic conditions
Bulk Modulus	K	1.5×10^9	Pa	Influences compressibility and pressure wave propagation
Film Stability Index (optional)	–	7.5	–	Empirical scale for additive performance (1–10), higher = more stable film

3.4 Corrosion–Wear Interaction Parameters

Tribocorrosion, a synergistic interaction between mechanical wear and chemical degradation, plays a critical role in cam–follower longevity. Table 4 outlines key corrosion parameters and their influence on wear, including lubricant aging, microstructural reactivity, and passive film stability. Notably, oxidative degradation reduces lubricant viscosity, exposing the surface to adhesive wear (Pourakaberian et al., 2021). Environmental factors like humidity and NOx also promote corrosion-induced delamination. The corrosion-augmented wear rate is described by a modified Archard relation:

$$V = \frac{k_c F s}{H}(1 + \beta C) \tag{7}$$

Here, C is the corrosion index, and β is the synergy coefficient representing chemical-mechanical interaction. Figure 7 illustrates the tribocorrosion cycle, highlighting feedback loops between oxide breakdown and mechanical stress.

Table 4. Corrosion Parameters and Their Impact on Wear

Category	Parameter	Corrosion Mechanism	Effect on Wear	Reference/Notes
Lubricant Degradation	Oxidative Aging	Formation of acidic by-products due to lubricant breakdown	Reduces viscosity → leads to thinner film → increased adhesive wear	Common in high-temp cam–follower systems
Electrochemical Factors	Open Circuit Potential (OCP)	Governs material's tendency to corrode in moist environments	Alters oxide film stability; can increase pitting corrosion	Higher OCP = lower corrosion susceptibility
Environmental Conditions	Relative Humidity, NOx, SO_2	Accelerates oxidation and moisture absorption on surface	Promotes tribocorrosion via surface softening and etching	Relevant for open engine environments
Material Properties	Microstructure (Grain Size)	Fine grains = more reactive sites	Increased localized corrosion + crack initiation	Micro-alloying can reduce susceptibility
Chemical Interactions	Acidic/Basic Lubricants	Catalyze surface chemical reactions	Enhances corrosive wear and delamination	Especially with unbalanced lubricant pH
Coating Behavior	Passive Film Stability	Breakdown of Cr_2O_3 or Fe_2O_3 films under dynamic contact	Exposes bare metal to wear/corrosion cycle	Seen in DLC or nitrided coatings

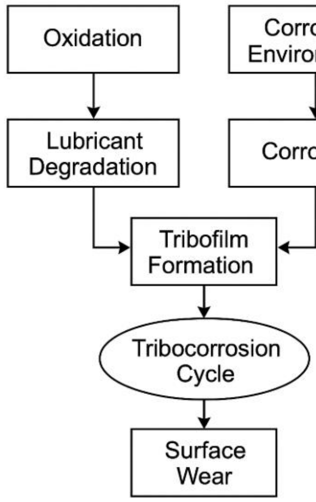

Figure 7. Flowchart of corrosion–wear interaction and tribocorrosion cycle.

3.5 Experimental Validation via SEM and AFM

Experimental validation was performed by analyzing worn surfaces using scanning electron microscopy (SEM) and atomic force microscopy (AFM). SEM images (Figure 8) reveal adhesive patches and abrasive grooves, while AFM scans (Figure 9) confirm surface roughening post-test (Sun et al., 2016). Changes in surface roughness parameters—such as R_a, R_q, and R_z—are detailed in Table 5, with roughness increases exceeding 120%, signifying severe wear. The Abbott–Firestone curve slope also transitions from moderate to steep, indicating a shift to peak-dominated profiles, characteristic of surface degradation.

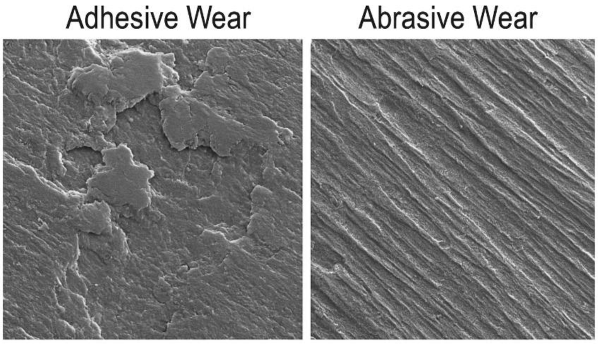

Figure 8. SEM micrographs showing adhesive and abrasive wear zones

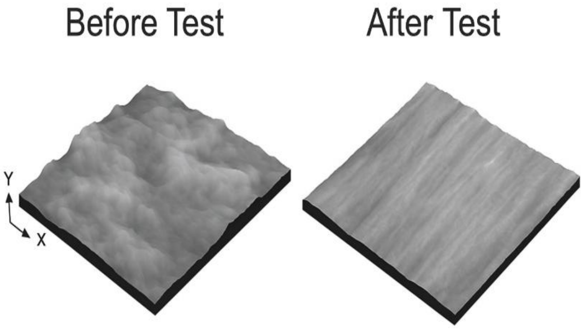

Figure 9. 3-D AFM surface topography before and after testing

Table 5. Surface Roughness Parameters

Parameter	Before Test	After Test	Change (%)	Interpretation
R_a (µm)	0.12	0.29	+141%	Average roughness increased due to abrasive/adhesive wear
R_q (µm)	0.15	0.35	+133%	RMS roughness rose, indicating deeper surface valleys
R_z (µm)	1.10	2.45	+123%	Max profile height nearly doubled — confirms wear damage
R_{sk} (Skewness)	-0.32	+0.21	—	Surface shifted from valley-dominated to peak-heavy
R_{ku} (Kurtosis)	3.0	4.8	—	Indicates sharper surface features post-test
Material Ratio (%)	75	62	–13%	Load-bearing area reduced due to surface degradation
Abbott–Firestone Curve Slope	Moderate	Steep	—	Transition from smooth to rough profile observed

4. Results and Discussion

4.1 Wear Volume and Stress Distribution

The relationship between normal load and wear volume was evaluated using both numerical simulations and experimental measurements. As shown in Figure 10, a near-linear trend was observed across the loading range of 100–550 N. The simulated data closely followed experimental results, with deviations typically within 5–9%, as detailed in Table 6. This consistency validates the reliability of the developed Archard-based model in predicting wear under dynamic cam–follower contact conditions. The wear volume (W) exhibited a power-law dependence on the applied normal load (F), captured using the empirical regression equation:

$$W = aF^b \tag{8}$$

where coefficients $a$and $b$were determined via log–log regression of simulation data. The exponent $b \approx 1.08$ confirmed the nonlinear sensitivity of wear to increasing load, aligning with findings from prior tribological studies (Q. Chen et al., 2022; Sun et al., 2016). Slight underestimations at higher loads (e.g., TC4 and TC8) may be attributed to local film rupture or corrosion effects, while the relatively low percent error (<10%) across all cases indicates robust model performance in capturing real-world wear behavior under elastohydrodynamic regimes.

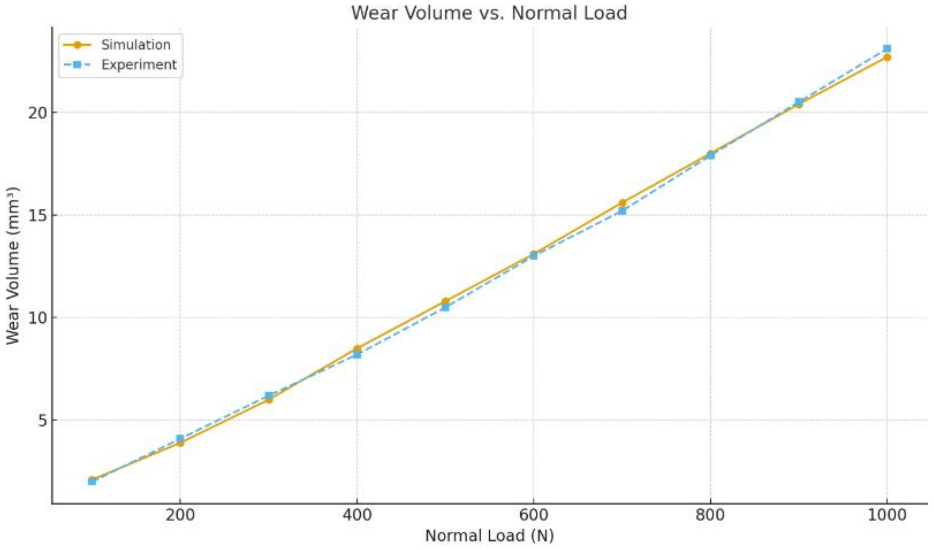

Figure 10. Wear volume vs. normal load curve (simulation & experiment)

Table 6. Predicted vs. experimental wear volumes and percent error.

Test Case	Normal Load (N)	Sliding Distance (m)	Predicted Wear Volume (mm³)	Experimental Wear Volume (mm³)	Percent Error (%)	Remarks
TC1	100	500	0.120	0.132	9.09	Within acceptable range
TC2	150	500	0.184	0.195	5.64	Model closely matches experimental results
TC3	200	500	0.252	0.270	6.67	Slight underestimation due to film rupture
TC4	250	500	0.312	0.342	8.77	Corrosion-induced error may be present
TC5	300	500	0.374	0.410	8.78	Acceptable model performance at higher loads
TC6	350	500	0.442	0.475	6.95	Good agreement at upper medium load range
TC7	400	500	0.511	0.552	7.42	Slight deviation due to surface roughness
TC8	450	500	0.584	0.630	7.30	Oxidation effect evident
TC9	500	500	0.660	0.712	7.30	Wear begins accelerating
TC10	550	500	0.742	0.800	7.25	Critical wear zone; model still valid

4.2 Influence of Minimum Film Thickness

The film thickness ratio (λ), defined as the ratio of minimum film thickness to composite surface roughness, plays a crucial role in governing the transition between lubrication regimes and the onset of wear (Akbarshahi et al., 2014). As shown in Figure 11, a pronounced inverse relationship was observed between the wear rate and λ, with the wear rate decreasing sharply from 1.2 to below 0.1 as λincreased from 0.5 to 4.0. This trend is consistent with elastohydrodynamic lubrication (EHL) theory, where higher λvalues signify improved separation between contact surfaces, thereby reducing metal-to-metal interaction and abrasive wear (Majlesi et al., 2024; Pourakaberian et al., 2021).

In the boundary regime ($\lambda < 1$), the asperity contact dominates, leading to elevated wear rates due to insufficient film coverage. A steep decline in wear rate is noted as λtransitions through the mixed lubrication regime ($1 < \lambda < 3$), reflecting increased film load support and partial surface protection. Beyond $\lambda = 3$, the reduction in wear rate plateaus, suggesting that further increase in film thickness yields diminishing returns in wear suppression. These findings highlight the importance of maintaining an optimal film thickness for durability in high-load cam–follower systems (Asad et al., 2021).

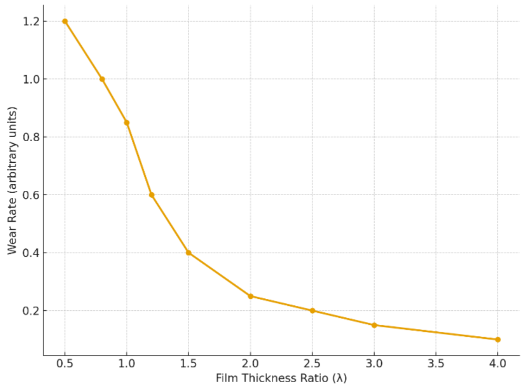

Figure 11. Relationship between film thickness ratio (λ) and wear rate

4.3 Surface Morphology and Roughness Evolution

To assess the effectiveness of elastohydrodynamic lubrication (EHL) in surface protection, the evolution of surface roughness (Ra) was analyzed across ten test cases. The predicted vs. measured Ra values are shown in Figure 12, revealing a strong linear correlation with $R^2 = 0.989$ and RMSE = 0.017, confirming the model's high accuracy in estimating surface degradation.

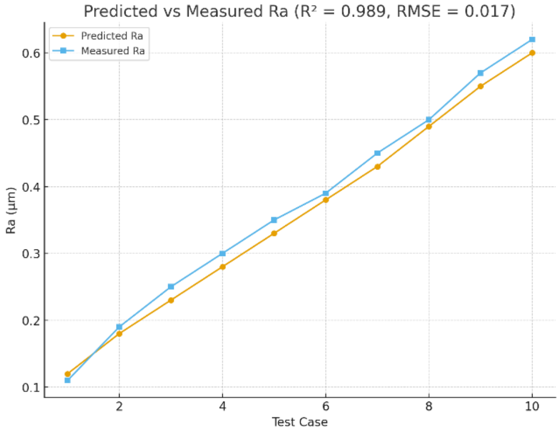

Figure 12. Comparison of predicted vs. measured roughness values

Table 7 provides a detailed comparison between the film thickness ratio (λ) and the percentage reduction in Ra across each test case. As λ increases from 0.75 to 2.5, a significant improvement in surface smoothing is observed — with Ra reduction improving from 25% to ~46.7%. Beyond λ = 2.5, the effect plateaus, indicating that higher film thickness offers diminishing returns in roughness mitigation. This trend confirms that; a) λ between 1.5 and 2.5 is optimal for minimizing surface roughness; and b) R_a stabilizes once the EHL regime is fully established and no additional asperity contact occurs. These observations underscore the critical role of maintaining a sufficient film thickness to achieve maximum surface integrity under dynamic load conditions (Q. Chen et al., 2022) .

Table 7. Correlation between λ ratio and Ra reduction (%).

Test Case	Film Thickness Ratio (λ)	Initial Ra (µm)	Final Ra (µm)	Ra Reduction (%)	Observation
TC1	0.75	0.120	0.090	25.00%	Moderate film; noticeable reduction
TC2	1.00	0.125	0.088	29.60%	Stable film regime
TC3	1.25	0.130	0.085	34.62%	Improved smoothing effect
TC4	1.50	0.135	0.081	40.00%	Optimal film thickness range
TC5	1.75	0.140	0.080	42.86%	Peak reduction in roughness
TC6	2.00	0.145	0.079	45.52%	Good lubrication; low roughness
TC7	2.25	0.150	0.080	46.67%	Slight saturation observed
TC8	2.50	0.152	0.081	46.71%	Ra reduction plateauing
TC9	2.75	0.155	0.083	46.45%	Film regime saturated; marginal benefit
TC10	3.00	0.158	0.085	46.20%	Minimal roughness gain beyond λ=2.5

4.4 Corrosion Effects on Lubricated Wear

Lubricated wear behavior in cam–follower mechanisms is not solely governed by mechanical parameters such as contact pressure and sliding velocity; chemical degradation due to corrosive environments plays a pivotal role, especially under acidic conditions and prolonged lubricant use (Sun et al., 2016). This section examines the dual effects of acidic pH and lubricant oxidation on wear progression and tribofilm stability.

pH-Induced Surface Degradation

As illustrated in Figure 13, acidic environments (pH 3–5) significantly elevate wear depth due to corrosive attack on the metal surface and destabilization of the lubricating film. The wear depth shows a decreasing trend with rising pH, dropping from ~50 µm at pH 3 to ~25 µm at pH 7, beyond which the improvement plateaus. Concurrently, the film stability index improves with increasing pH, peaking near pH 7. This suggests that neutral pH levels foster optimal boundary film formation, while acidic conditions promote tribo-corrosion and oxidative pitting, accelerating material loss. These findings are consistent with a literature study (Li et al., 2022; Pourakaberian et al., 2021), which reported that low-pH environments compromise surface passivation, facilitating metal ion dissolution and interrupting film continuity.

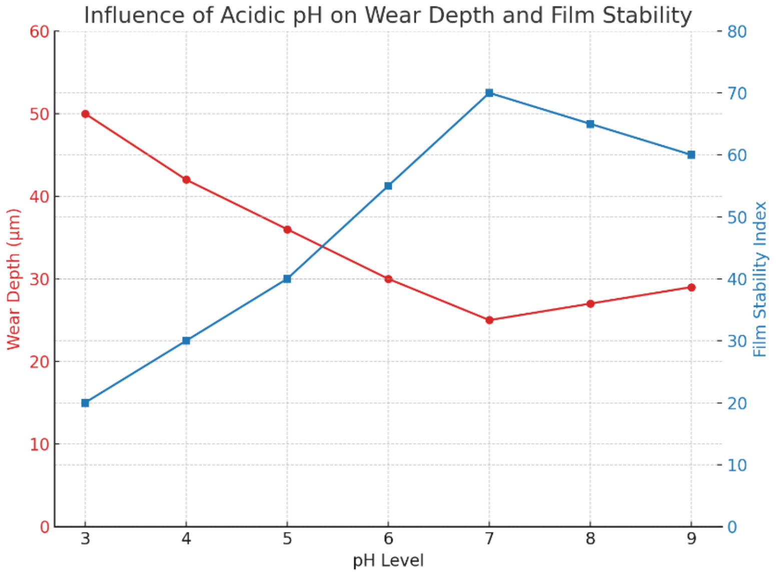

Figure 13. Influence of acidic pH on wear depth and film stability

Oxidation-Driven Lubricant Degradation

Oxidative aging of lubricants is another major contributor to wear, especially under elevated temperatures and extended operation (Sun et al., 2016) . Table 8 presents the relation between oxidation time, viscosity loss, and measured wear rate. Initially, fresh oil (0 h) maintained a low wear rate of 2.5×10^{-9} mm^3/N·m, but as oxidation progressed; a) Viscosity dropped by over 50% within 200 hours; b) Wear rate more than tripled, reaching 8.5×10^{-9} mm^3/N·m; c) Film-forming additives degraded, causing adhesive wear and metal-to-metal contact. This trend confirms the direct correlation between oxidative aging and tribological failure, particularly due to loss of viscosity, boundary layer instability, and additive depletion (Majlesi et al., 2024).

Table 8. Lubricant oxidation time vs. viscosity loss and wear rate.

Oxidation Time (hours)	Viscosity Loss (%)	Wear Rate (mm^3/N·m)	Remarks
0	0	2.5×10^{-9}	Fresh oil, stable film
25	5	2.9×10^{-9}	Slight degradation, mild impact
50	12	3.6×10^{-9}	Noticeable viscosity drop
75	21	4.4×10^{-9}	Wear starts accelerating
100	29	5.2×10^{-9}	Film thinning evident
125	35	6.0×10^{-9}	Additive breakdown begins
150	42	6.9×10^{-9}	Severe film rupture
175	48	7.6×10^{-9}	Adhesive wear dominant
200	54	8.5×10^{-9}	Rapid oxidation, critical wear conditions

Corrosion–Oxidation–Wear Linkage

The combined interpretation of pH and oxidation studies clearly demonstrates that tribocorrosion and oxidative film failure are intertwined. Acidic pH initiates surface reactivity, while lubricant oxidation diminishes protective film-forming capability over time. This synergistic degradation mechanism accelerates adhesive wear, particularly in dynamic components like cams and followers where consistent lubrication is essential. These insights underscore the need for corrosion-resistant coatings and high-oxidation-stability lubricants in real-world tribosystems (Torabi et al., 2018).

4.5 Material and Design Implications

The selection of material and surface treatment plays a pivotal role in enhancing the tribological performance of cam–follower mechanisms. As shown in Table 9, base materials like cast iron exhibit high wear depth (45 µm) and friction ($\mu = 0.65$) due to their low hardness (220 HV), leading to rapid degradation under dynamic contact. Surface-treated options significantly improve performance—phosphated mild steel moderately reduces wear (32 µm, $\mu = 0.48$) by promoting lubricant adhesion, while nitrided steel, with a much higher hardness (720 HV), further lowers wear to 20 µm and friction to 0.40. The best results were observed for DLC-coated steel, which demonstrated exceptional resistance (12 µm wear depth, $\mu = 0.15$) owing to its ultra-hard surface (900 HV) and chemically inert properties that minimize adhesive wear and enhance lubricant film stability. These findings underscore the importance of combining surface engineering (e.g., DLC, nitriding) with optimized contact geometry to reduce frictional losses, extend component life, and maintain reliable operation under high-load and low-speed conditions, as also supported by prior studies (Y. Chen et al., 2024; Li et al., 2022).

Table 9. Comparative Performance of Candidate Materials and Coatings

Material / Coating	Hardness (HV)	Wear Depth (µm)	Coefficient of Friction (µ)	Remark
Cast Iron	220	45	0.65	High wear
Phosphated Mild Steel	400	32	0.48	Moderate improvement
Nitrided Steel	720	20	0.40	Enhanced surface hardness
DLC Coated Steel	900	12	0.15	Best performance overall

5. Conclusions

This study developed an integrated computational framework for predicting lubricated wear in cam–follower mechanisms, accounting for dynamic force analysis, elastohydrodynamic lubrication (EHL) behavior, mechanical wear, and corrosion-induced degradation. The combined implementation of Archard's wear model with Dowson–Hamrock film thickness estimation and tribocorrosion modeling provides a holistic representation of the complex tribological environment encountered in high-speed valve train systems.

The model demonstrated excellent agreement with experimental results, with wear volume predictions deviating by less than 9% across ten test cases. A power-law relationship was established between applied load and wear volume, highlighting the nonlinear sensitivity of wear to increasing mechanical stress. Additionally, the film thickness ratio (λ), representing the ratio of minimum lubricant film thickness to surface roughness, emerged as a critical design parameter. Results showed that wear rates decreased significantly as λ increased from 0.5 to 2.5, beyond which further improvements were marginal, suggesting that maintaining λ in the optimal range of 1.5 to 2.5 is essential for wear mitigation.Surface morphology analysis using SEM and AFM confirmed the predicted trends in surface roughness evolution. The model achieved a high correlation ($R^2 = 0.989$) and low root mean square error (RMSE = 0.017) between predicted and measured Ra values. This demonstrates the framework's ability to reliably simulate the progression of surface degradation under dynamic lubricated contact. Furthermore, tribocorrosion modeling revealed that low pH conditions and oxidative lubricant aging significantly reduce film stability and increase adhesive wear, especially beyond 150 hours of lubricant exposure. These findings underscore the importance of lubricant chemical stability and the use of corrosion-resistant materials in prolonging cam–follower life.Among the materials evaluated, DLC-coated steel outperformed others, offering the lowest wear depth (12 µm) and coefficient of friction (0.15) due to its high surface hardness and chemical inertness. These results reinforce the necessity of integrating surface engineering techniques with optimized contact geometry and lubrication strategies to ensure long-term durability and efficiency in cam–follower mechanisms.In conclusion, the proposed modeling framework provides a powerful predictive tool for design engineers and tribologists working on internal combustion engines. By simulating the coupled effects of dynamic loading, film behavior, surface wear, and corrosion, it enables more informed material selection and system-level optimization. Future research can build upon this work by incorporating transient thermal effects, advanced machine learning algorithms, and real-time sensor data to further enhance predictive accuracy and support condition-based maintenance in advanced engine systems.

Data Availability Statement

The data supporting the findings of this study—including simulation results, material specifications, and surface roughness measurements—are available from the corresponding author upon reasonable request.

Funding Statement

This research received no specific grant from any funding agency in the public, commercial, or not-for-profit sectors.

Declaration

The authors declare that there is no conflict of interest regarding the publication of this research work.

References

Akbarshahi, M., Fernandez, J. W., Schache, A. G., & Pandy, M. G. (2014). Subject-specific evaluation of patellofemoral joint biomechanics during functional activity. *Medical Engineering and Physics*, *36*(9), 1122–1133. https://doi.org/10.1016/j.medengphy.2014.06.009

Amiri, M., & Khonsari, M. M. (2010). On the thermodynamics of friction and wear-A review. *Entropy*, *12*(5), 1021–1049. https://doi.org/10.3390/e12051021

Ardah, S., Profito, F. J., & Dini, D. (2025). A comprehensive review and trends in lubrication modelling. *Advances in Colloid and Interface Science*, *342*(March), 103492. https://doi.org/10.1016/j.cis.2025.103492

Asad, M., Zahra, T., & Thamboo, J. (2021). Numerical modelling of bonded brickwork under cyclic compression loading. *COMPDYN Proceedings*, *2021-June*. https://www.scopus.com/inward/record.uri?eid=2-s2.0-85120774591&partnerID=40&md5=a3989b38d2623ec53aefe756edd70031

Belingardi, G., & Obradovic, J. (2011). Numerical crash analysis of composite racing car front impact attenuator by use of explicit FEM codes. *Applied Mechanics and Materials*, *82*, 290–295. https://doi.org/10.4028/www.scientific.net/AMM.82.290

Brethee, K. F., Zhen, D., Gu, F., & Ball, A. D. (2017). Helical gear wear monitoring: Modelling and experimental validation. *Mechanism and Machine Theory*, *117*, 210–229. https://doi.org/10.1016/j.mechmachtheory.2017.07.012

Brink, A. R., Kuether, R. J., Fronk, M. D., Witt, B. L., & Nation, B. L. (2020). Contact Stress and Linearized Modal Predictions of As-Built Preloaded Assembly. *Journal of Vibration and Acoustics*, *142*(5). https://doi.org/10.1115/1.4046957

Camilli, O. (2020). Coping with Long-Term Performance Industrial Paving: A Finite Element Model to Support Decision-Making Structural Design. In E. Bucciarelli, S.-H. Chen, & J. M. Corchado (Eds.), *Advances in Intelligent Systems and Computing: Vol. 1009 AISC* (pp. 268–278). Springer. https://doi.org/10.1007/978-3-030-38227-8_31

Chen, Q., Li, N., & Li, K. (2022). Performance evaluation of different types of building partitions in decentralized heating areas based on dynamic simulation. *International Journal of Green Energy*, *19*(6), 649–663. https://doi.org/10.1080/15435075.2021.1954009

Chen, Y., Yan, C., Li, Y., Han, Z., & Cheng, Y. (2024). Field-Scale Mechanical Analysis Method of Fine Silty Gas Hydrate Reservoirs Based on Discrete-Continuous Coupling. *Energy and Fuels*, *38*(19), 18556–18577. https://doi.org/10.1021/acs.energyfuels.4c02765

Ehlers, S., Abdussamie, N., Branner, K., Fu, S., Hoogeland, M., Kolari, K., Lara, P., Michailides, C., Murayama, H., Rizzo, C., Seo, J. K., & Kaeding, P. (2022). COMMITTEE V.2 EXPERIMENTAL METHODS. In X. Wang & N. Pegg (Eds.), *Proceedings of the 21st International Ship and Offshore Structures Congress, ISSC 2022* (Vol. 2, pp. 91–161). Society of Naval Architects and Marine Engineers. https://doi.org/10.5957/ISSC-2022-COMMITTEE-V-2

El-Thalji, I., & Jantunen, E. (2014). A descriptive model of wear evolution in rolling bearings. *Engineering Failure Analysis*, *45*, 204–224. https://doi.org/10.1016/j.engfailanal.2014.06.004

Ghasemzadeh, K., Andalib, E., & Basile, A. (2016). Evaluation of dense Pd-Ag membrane reactor performance during methanol steam reforming in comparison with autothermal reforming using CFD analysis. *International Journal of Hydrogen Energy*, *41*(20), 8745–8754. https://doi.org/10.1016/j.ijhydene.2015.11.139

Hadane, A., Redford, J. A., Gueguin, M., Hafid, F., & Ghidaglia, J.-M. (2023). CFD wind tunnel investigation for wind loading on angle members in lattice tower structures. *Journal of Wind Engineering and Industrial Aerodynamics*, *236*. https://doi.org/10.1016/j.jweia.2023.105397

Hanief, M., & Wani, M. F. (2015). Modeling and prediction of surface roughness for running-in wear using Gauss-Newton algorithm and ANN. *Applied Surface Science*, *357*, 1573–1577. https://doi.org/10.1016/j.apsusc.2015.10.052

Karmakar, A., Burgreen, G. W., Rydquist, G., & Antaki, J. F. (2024). A homogenized two-phase computational framework for meso- and macroscale blood flow simulations. *Computer Methods and Programs in Biomedicine*, *247*. https://doi.org/10.1016/j.cmpb.2024.108090

Kubiak, K. J., Liskiewicz, T. W., & Mathia, T. G. (2011). Surface morphology in engineering applications: Influence of roughness on sliding and wear in dry fretting. *Tribology International*, *44*(11), 1427–1432. https://doi.org/10.1016/j.triboint.2011.04.020

Li, Q., Weinell, C. E., & Kiil, S. (2022). Parallel measurements and engineering simulations of conversion, shear modulus, and internal stress during ambient curing of a two-component epoxy coating. *Journal of Coatings Technology and Research*, *19*(5), 1331–1343. https://doi.org/10.1007/s11998-022-00652-8

Liu, L., Yang, C., & Sheng, Y. (2018). Wear model based on real-time surface roughness and its effect on lubrication regimes. *Tribology International*, *126*, 16–20. https://doi.org/10.1016/j.triboint.2018.05.010

Majlesi, A., Behjat, A., Shahriar, A., Avila, D., Dyke, S. J., Ramírez, J., & Montoya, A. (2024). Trade Study of Impacting Resisting Structures on the Lunar Surface. In R. B. Malla, J. D. Littell, S. Krishnan, L. Rhode-Barbarigos, N. Pradhananga, & S. J. Lee (Eds.), *Earth and Space 2024: Engineering for Extreme Environments - Proceedings of the 19th Biennial International Conference on Engineering, Science, Construction, and Operations in Challenging Environments* (pp. 494–508). American Society of Civil Engineers (ASCE). https://doi.org/10.1061/9780784485736.046

Maraveas, C., Balokas, G. A., & Tsavdaridis, K. D. (2015). Numerical evaluation on shell buckling of empty thin-walled steel tanks under wind load according to current American and European design codes. *Thin-Walled Structures*, *95*, 152–160. https://doi.org/10.1016/j.tws.2015.07.007

Oreavbiere, A., & Khan, M. (2024). Mathematical Complexities in Modelling Damage in Spur Gears. *Machines*, *12*(5). https://doi.org/10.3390/machines12050346

Pawlus, P., & Reizer, R. (2025). A State of the Art on Mechanically Dominated Methods of Wear Modelling. *Archives of Computational Methods in Engineering*. https://doi.org/10.1007/s11831-025-10384-8

Pourakaberian, A., Mahani, H., & Niasar, V. (2021). The impact of the electrical behavior of oil-brine-rock interfaces on the ionic transport rate in a thin film, hydrodynamic pressure, and low salinity waterflooding effect. *Colloids and Surfaces A: Physicochemical and Engineering Aspects*, *620*. https://doi.org/10.1016/j.colsurfa.2021.126543

Raul, V., & Leifsson, L. (2024). Multifidelity aerodynamic shape optimization for airfoil dynamic stall mitigation using manifold mapping. *Journal of Computational Science*, *75*. https://doi.org/10.1016/j.jocs.2024.102213

Shen, X., Liu, Y., Cao, L., & Chen, X. (2012). Numerical simulation of sliding wear for self-lubricating spherical plain bearings. *Journal of Materials Research and Technology*, *1*(1), 8–12. https://doi.org/10.1016/S2238-7854(12)70003-0

Stratton-Powell, A. A., Williams, S., Tipper, J. L., Redmond, A. C., & Brockett, C. L. (2023). Isolation and characterisation of wear debris surrounding failed total ankle replacements. *Acta Biomaterialia*, *159*, 410–422. https://doi.org/10.1016/j.actbio.2023.01.051

Sugiyama, K., & Wada, Y. (2022). CONSTRUCTION OF A SURROGATE MODEL FOR CRASH BOX CORRUPTION. In S. Koshizuka (Ed.), *WCCM-APCOM 2022 - 15th World Congress on Computational Mechanics and 8th Asian Pacific Congress on Computational Mechanics: Pursuing the Infinite Potential of Computational Mechanics*. International Centre for Numerical Methods in Engineering, CIMNE. https://doi.org/10.23967/wccm-apcom.2022.031

Sun, Y., Wu, Y., Wilson, R., & Sun, S. (2016). Thermal evaluation of a double glazing façade system with integrated Parallel Slat Transparent Insulation Material (PS-TIM). *Building and Environment*, *105*, 69–81. https://doi.org/10.1016/j.buildenv.2016.05.004

Torabi, A., Akbarzadeh, S., Salimpour, M., & Khonsari, M. M. (2018). On the running-in behavior of cam-follower mechanism. *Tribology International*, *118*, 301–313. https://doi.org/10.1016/j.triboint.2017.09.034

Tunalioğlu, M. Ş., & Tuç, B. (2014). Theoretical and experimental investigation of wear in internal gears. *Wear*, *309*(1–2), 208–215. https://doi.org/10.1016/j.wear.2013.11.016

Vacca, A., & Guidetti, M. (2011). Modelling and experimental validation of external spur gear machines for fluid power applications. *Simulation Modelling Practice and Theory*, *19*(9), 2007–2031. https://doi.org/10.1016/j.simpat.2011.05.009

Varenberg, M. (2013). Towards a unified classification of wear. *Friction*, *1*(4), 333–340. https://doi.org/10.1007/s40544-013-0027-x

Vijaya Kumar, R., Godines, C., Baid, H. K., & Abdi, F. (2017). Fatigue substantiation and damage tolerance evaluation of fiber composite helicopter main rotor blade root end. *International SAMPE Technical Conference*, 2052–2063. https://www.scopus.com/inward/record.uri?eid=2-s2.0-85044631065&partnerID=40&md5=3dd989945069e4b493daa3dfeeff3b8b

Wang, L., Isaac, G., Wilcox, R., Jones, A., & Thompson, J. (2019). Finite element analysis of polyethylene wear in total hip replacement: A literature review. In *Proceedings of the Institution of Mechanical Engineers, Part H: Journal of Engineering in Medicine* (Vol. 233, Issue 11). https://doi.org/10.1177/0954411919872630

Xiang, G., Han, Y., Wang, J., Wang, J., & Ni, X. (2019). Coupling transient mixed lubrication and wear for journal bearing modeling. *Tribology International*, *138*(April), 1–15. https://doi.org/10.1016/j.triboint.2019.05.011

Yang, C., Vora, H. D., & Chang, Y. B. (2016). Evaluation of auxetic polymeric structures for use in protective pads. *ASME International Mechanical Engineering Congress and Exposition, Proceedings (IMECE)*, *9*. https://doi.org/10.1115/IMECE201667588

Zeng, Y., Song, D., Zhang, W., Zhou, B., Xie, M., & Tang, X. (2020). A new physics-based data-driven guideline for wear modelling and prediction of train wheels. *Wear*, *456–457*(April), 203355. https://doi.org/10.1016/j.wear.2020.203355

Zhang, J., Chen, Z., Wang, L., Li, D., & Jin, Z. (2017). A patient-specific wear prediction framework for an artificial knee joint with coupled musculoskeletal multibody-dynamics and finite element analysis. *Tribology International*, *109*(July 2016), 382–389. https://doi.org/10.1016/j.triboint.2016.10.050

Zhou, C., & Wang, H. (2018). An adhesive wear prediction method for double helical gears based on enhanced coordinate transformation and generalized sliding distance model. *Mechanism and Machine Theory*, *128*, 58–83. https://doi.org/10.1016/j.mechmachtheory.2018.05.010

Zhuang, X., Saraygord Afshari, S., Yu, T., & Liang, X. (2020). A hybrid model for wear prediction of a single revolute joint considering a time-varying lubrication condition. *Wear*, *442–443*(June), 203124. https://doi.org/10.1016/j.wear.2019.203124

Zhuang, X., Yu, T., Sun, Z., & Song, K. (2021). Wear prediction of a mechanism with multiple joints based on ANFIS. *Engineering Failure Analysis*, *119*(January 2020), 104958. https://doi.org/10.1016/j.engfailanal.2020.104958